Scientia Iranica F (2021) 28(6), 3753–3766

SCIENTIA IRANICA

Sharif University of Technology
Scientia Iranica
Transactions F: Nanotechnology
http://scientiairanica.sharif.edu

Effects of heat and mass transfer on stagnation point flow of micropolar Maxwell fluid over Riga plate

S. Nadeem[a], A. Amin[a], N. Abbas[a], A. Saleem[b,c,*], F.M. Alharbi[d], A. Hussain[a], and A. Issakhov[e]

a. *Department of Mathematics, Quaid-I-Azam University 45320, Islamabad 44000, Pakistan.*
b. *Mathematics and Its Applications in Life Sciences Research Group, Ton Duc Thang University, Ho Chi Minh City, Vietnam.*
c. *Faculty of Mathematics and Statistics, Ton Duc Thang University, Ho Chi Minh City, Vietnam.*
d. *Department of Mathematics, Faculty of Science, University of Tabuk, P.O. Box 741, Tabuk 71491, Saudi Arabia.*
e. *Al-Farabi Kazakh National University, av. al-Farabi 71, 050040, Almaty, Kazakhstan.*

Received 24 June 2019; received in revised form 2 September 2020; accepted 23 August 2021

KEYWORDS
Micropolar viscoelasticity fluid;
Multi-dependent thermophoresis;
Stagnation point flow;
Riga plate;
Numerical technique.

Abstract. In this paper, we investigated the stagnation point flow of Maxwell micropolar fluid flow over a Riga plate. Micropolar fluid flows over the Riga plate were used to create the mathematical model. The system of partial differential equations is created using the momentum equation and the micro inertia theory to accomplish the boundary layer approximation. Through appropriate similarity transformations, nonlinear partial differential equations are transformed into dimensionless nonlinear ordinary differential equations. This system solved the numerical scheme via the BVP4C method. The effects of involving physical parameters like dimensionless parameter, modified Hartman number, material parameter, slip condition σ_s, viscoelastic parameter δ_m and Soret coefficient S_T are shown through graphs and numerical results. The physical quantities such as Skin friction, local Nusselt number, and local Sherwood number are shown in tables. R increases when the dimensionless parameter, Material parameter K and Slip condition σ_s increase, while R decreases with the Modified Hartman number Z and viscoelastic parameter δ_m increase.

1. Introduction

Micropolar fluid analysis has a significant impact on engineering and industrial processes. In comparison to Newtonian fluids, micropolar fluids have a strong resistance to fluid motion. Because of its potential applications, many researchers with varied preconceptions are interested in studying the micropolar fluid. Lukaszewicz [1] studied the micropolar fluid theory and its applications in the early stages of his career. Eringen extended the theory of Lukaszewicz [2]. He introduced the micropolar fluids Microcontinuum field theory. Several traditional assumptions, such as the absence of couple stress or the symmetry of the stress tensor, have never been proven. Because of its relative simplicity in mathematics, the micropolar fluid model has been widely employed in lubricants to examine polymer clarifications in which the viscous fluid lubricant is merged with a little amount of long-chain extra substances. The effects of lubricating on the micropolar fluid were studied by Wang and Zhu [3]. They analyzed the basic theory of micropolar fluid and derived the modified Reynolds equation for dynamics

*. *Corresponding author.*
E-mail address: anber.saleem@tdtu.edu.vn (A. Saleem)

doi: 10.24200/sci.2021.53858.3454

loads. Because of the wide range of applications, several researchers have investigated micropolar fluids thoroughly from various perspectives. The numerical and exact solutions of micropolar fluids in the vertical annulus were obtained by Nadeem et al. [4]. The micropolar fluid over the stretching sheet was explored by Hussain et al. [5]. Ellahi et al. [6] studied heat and mass transfer of micropolar fluid over permeable walls. The mixed convection flow with heat transfer of micropolar nanofluid was investigated by Rawi et al. [7]. Abbas et al. [8] investigated the nanomaterial micropolar fluid in the cylinder. They also studied the effects of thermal slip and velocity slip on micropolar nanofluid. The behavior of micropolar fluid on Riga plate was studied by Nadeem et al. [9]. Many researchers are interested in investigating the characteristics of various physical parameters of micropolar fluid (see [10–13]).

Electromagnetic forces can control the flow of fluid since it is electrically conductive. An attractive hydrodynamics flow control can often be used to regulate the speed of liquids with high electrical conductivity. In the case of a feebly conducting liquid, the current created by the outside attractive field alone is extremely little, whereas the outside electric field must be coupled to pick up an effective stream control. The first researchers who investigated the Riga plate were Gailitis and Lielausis [14]. They developed the Riga plate; a device that creates crossed magnetic and electric fields. The properties of a few potential fields were studied by Grinberg [15]. As shown by Grinberg [15], the divider parallel Lorentz drive within the boundary layer force condition is completely decoupled from the stream and stood in the opposite situation with respect to the Hartmann term. Along the plate, it decreases exponentially. The boundary layer flow across the Riga plate was investigated by Pantokratoras and Magyari [16]. The opposing and aiding mixed convection flow over the Riga plate was studied by Magyari and Pantokratoras [17]. Under the modified Hartmann number, Ayub et al [18] studied the Blasius flow over the Riga plate. The effects of nanomaterial micropolar fluid flow on the Riga plate were studied by Ramzan et al. [19]. Zaib et al. [20] investigated the mixed convective condition of micropolar fluid flow across the Riga plate. Rasool and Zhang [21] investigated the convective boundary conditions and chemical radiations on the Riga plate. Because of its limited applications in engineering, as indicated in [22–27], few researchers have focused on the Riga plate.

Hiemenz [28] was the first researcher who introduced stagnation flow to gain the exact solution of the Navier-Stokes equations. Howarth [29] examined the Hiemenz [28] idea and found the best solution approximations. Ishak et al. [30] studied the boundary layer flow with the magnetic field effects in the stagnation point region. Van Gorder and Vajravelu [31] investigated the stagnation point flow of second-grade fluid over a stretching surface. Fang et al. [32] investigated the unsteady stagnation point flow with mass transfer. Recent studies on the stagnation point flows are presented in [33–41].

We investigated the stagnation point flow of Maxwell viscoelasticity with incompressible micropolar fluid over the Riga plate. The mathematical model has been constructed using micropolar fluid flows over the Riga plate. The system of partial differential equations used to perform the boundary layer approximation is created using the momentum equation and micro inertia theory. Through appropriate similarity transformations, nonlinear partial differential equations can be transformed into dimensionless nonlinear ordinary differential equations. This system solved numerical scheme via the BVP4C method. Analysis of physical parameters of the Riga plate results is shown in form of tables and figures.

2. Formulation of flow

We examined the two-dimensional Maxwell Viscoelasticity-based Micropolar Fluid (MVMF) in the stagnation point on the horizontal Riga plate with slip velocity condition as shown in Figure 1. The plate was in the direction of X-axis as well as normal to plate id Y-axis. We defined $U_w = ax$ as the linear velocity on the wall and a as the positive constant. In mathematics, a flow model can be written as:

$$\frac{\partial u}{\partial x}+\frac{\partial v}{\partial y}=0, \tag{1}$$

$$u\frac{\partial u}{\partial x}+v\frac{\partial u}{\partial y}=\lambda\bar{U}_e^2\frac{d^2\bar{U}_e}{d\bar{x}^2}+\bar{U}_e\frac{d\bar{U}_e}{d\bar{x}}+\left(\frac{\mu+\kappa}{\rho}\right)\frac{\partial}{\partial y}\left(\frac{\partial u}{\partial y}\right) -\lambda\left(u^2\frac{\partial^2 u}{\partial x^2}+v^2\frac{\partial^2 u}{\partial y^2}+2uv\frac{\partial^2 u}{\partial x\partial y}\right) +\frac{\kappa}{\rho}\frac{\partial N}{\partial y}+\frac{\pi j_0 M_0}{8\rho}e^{\frac{-\pi}{b}y}, \tag{2}$$

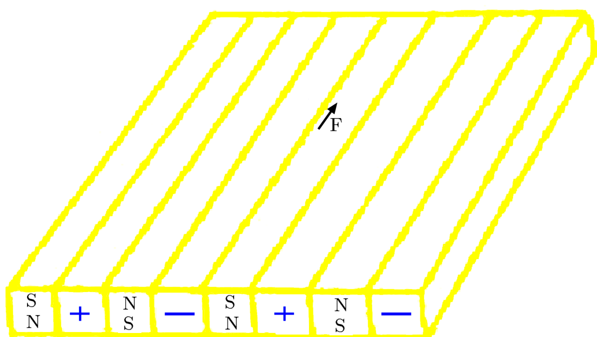

Figure 1. Physical configuration of the flow.

where the free steam velocity is $U_e = \omega x$ and ω is the positive constant:

$$u\frac{\partial u}{\partial x}+v\frac{\partial u}{\partial y}=\omega^2 x+\left(\frac{\mu+\kappa}{\rho}\right)\frac{\partial}{\partial y}\left(\frac{\partial u}{\partial y}\right)-\lambda\left(u^2\frac{\partial^2 u}{\partial x^2}+v^2\frac{\partial^2 u}{\partial y^2}+2uv\frac{\partial^2 u}{\partial x\partial y}\right)+\frac{\kappa}{\rho}\frac{\partial N}{\partial y}+\frac{\pi j_0 M_0}{8\rho}e^{\frac{-\pi}{b}y}, \tag{3}$$

$$\rho j\left(u\frac{\partial N}{\partial x}+v\frac{\partial N}{\partial y}\right)=\frac{\partial}{\partial y}\left(\gamma\frac{\partial N}{\partial y}\right)-\kappa\left(2N+\frac{\partial u}{\partial y}\right). \tag{4}$$

Here, u and v are axial and transverse velocity components, respectively, μ is dynamic viscosity, κ is gyro-viscosity or vortex viscosity, ρ is the density of the fluid, N is micro-angular velocity and rotation is normal to plate along $x-y$ sheet, $\lambda=\frac{\alpha}{\rho}$ is relaxation time (T), in which α is the thermal diffusivity, M_0 is permanent magnets namely magnetization, j_0 is current density, b is electrodes and magnet width, j is micro-inertia per unit mass $\left(j=\frac{\nu}{\omega}\right)$, and γ is spin gradient viscosity which represents the relationship between μ and j and can be written as:

$$\gamma=\left(\mu+\frac{\kappa}{2}\right)j=\mu\left(1+\frac{K}{2}\right)j. \tag{5}$$

Here $K=\frac{\kappa}{\mu}$ represents dimensionless ratio of viscosity and is known as MVMF material parameter. The slip boundary on the surface is defined as:

$$u=u_w+u_{slip},\quad v=0,\quad N=-m\frac{\partial u}{\partial y},\quad \text{at}\quad y=0. \tag{6}$$

The condition at infinity is defined as:

$$u\rightarrow U_e=\omega x,\quad N\rightarrow 0\quad \text{as}\quad y\rightarrow\infty, \tag{7}$$

where u_{slip} is the slip velocity which is defined as $u_{slip}=L\Big[(1+K)\frac{\partial u}{\partial y}+KN\Big]_{y=0}$ in which $L=l\mu$ is a positive constant; m is a constant lying between 0 and 1, where $m=0$ indicates the concentrated MVMF and $m=0$ represents turbulent flow circumstance. In our case, we use $m=\frac{1}{2}$ to define a *dilute* MVMF.

3. Mathematical model of heat and mass transfer

We suppose that the surface temperature of the Riga plate is T_w while the temperature in a free-stream condition, also known as the ambient temperature, is T_∞ where $T_w > T_\infty$. Here C_w is the concentration of the plate on the surface and C_∞ is ambient concentration. By using the above assumptions and boundary layer principle, we obtain conservations equations of energy and concentration equation for MVMF:

$$u\frac{\partial T}{\partial x}+v\frac{\partial T}{\partial y}=\frac{k}{\rho C_p}\frac{\partial^2 T}{\partial y^2}+\frac{k_T D_m}{C_s C_p}\frac{\partial^2 C}{\partial y^2}+\frac{\mu_B+\kappa}{\rho C_p}\left(\frac{\partial u}{\partial y}\right)^2, \tag{8}$$

$$u\frac{\partial C}{\partial x}+v\frac{\partial C}{\partial y}=D_m\frac{\partial^2 C}{\partial y^2}+\frac{k_T D_m}{T_m}\frac{\partial^2 T}{\partial y^2}. \tag{9}$$

Corresponding boundary conditions are as follows:

$$T=T_w,\quad C=C_w\quad \text{at}\quad y=0, \tag{10}$$

$$T=T_\infty,\quad C=C_\infty\quad \text{as}\quad y\rightarrow\infty, \tag{11}$$

where:

k	Thermal conductivity of the fluid
D_m	Mass diffusivity
T_m	Fluid temperature across the boundary layer
C_s	Concentration susceptibility
k_T	Thermal diffusion ratio
C_p	Specific heat capacity

4. Similarity transformation equation

We have introduced the following suitable similarity transformation:

$$\psi=(\omega v)^{\frac{1}{2}}xf(\eta),\quad \eta=\left(\frac{\omega}{v}\right)^{\frac{1}{2}}y,\quad N=\left(\frac{\omega^3}{v}\right)^{\frac{1}{2}}xR, \tag{12}$$

$$\theta=\frac{T-T_\infty}{T_w-T_\infty},\qquad \phi=\frac{C-C_\infty}{C_w-C_\infty}. \tag{13}$$

The velocity components are expressed as follows:

$$u=\frac{\partial\psi}{\partial y},\qquad v=-\frac{\partial\psi}{\partial x}, \tag{14}$$

where η is non-dimensional parameter, R is non-dimensional local microvelocity, $v=\frac{\mu}{\rho}$ is kinematic viscosity, θ is the normalized temperature and ϕ is normalized concentration. By means of similarity transformation equations, Eqs. (3)–(4) and (8)–(9) are reduced as follows:

$$(1+K)f'''+ff''-(f')^2-\delta_m\left(1+f^2f'''-2ff'f''\right)+KR'+Ze^{-d\eta}+1=0, \tag{15}$$

$$\left(1+\frac{K}{2}\right)R''+fR'-f'R-K\left(2R+f''\right)=0, \tag{16}$$

$$\frac{1}{Pr}\theta''+f\theta'+Du\phi''+Gb\left(1+K\right)\left(f''\right)^2=0, \quad (17)$$

$$\phi''+Sc\left(f\phi'+Sr\theta''\right)=0. \quad (18)$$

Corresponding non-dimensional boundary conditions are:

$$f\left(0\right)=0, \qquad f'\left(0\right)=S+\sigma_s\left(1+\frac{K}{2}\right)f''\left(0\right),$$

$$R\left(0\right)=-\frac{f''\left(0\right)}{2}, \quad (19)$$

$$\theta\left(0\right)=1, \qquad \phi\left(0\right)=1, \quad (20)$$

$$f'\left(\infty\right)=1, \qquad R\left(\infty\right)=0, \qquad \theta\left(\infty\right)=0,$$

$$\phi\left(\infty\right)=0. \quad (21)$$

Here prime represents derivative with respect to η, $\delta_m=\lambda\omega$ denotes the non-dimensional viscoelastic parameter, Pr is Prandtl number, $Pr=\frac{\mu C_p}{\kappa}$, σ_s is the slip velocity parameter, $\sigma_s=l(\rho\mu\omega)^{\frac{1}{2}}$ is Gebhart number defined as Gb, Sc is Schmidt number, $Sc=\frac{v}{D_m}$, Du is the Dufour number, $Du=\frac{k_T D_m(C_w-C_\infty)}{C_s C_p v(T_w-T_\infty)}$, Sr is Soret number defined as $Sr=\frac{k_T D_m(T_w-T_\infty)}{T_m v(C_w-C_\infty)}$, Z is the modified Hartman number defined as $Z=\frac{\pi j_0 M_0 x}{8\rho U_e^2}$, and d is dimensionless parameter, $d=\frac{\pi}{b}\sqrt{\frac{v}{\omega}}$. For stretching we have $\left(S=\frac{a}{\omega}>0\right)$ and for shrinking we have $\left(S=\frac{a}{\omega}<0\right)$,

where:

S	stretching/shrinking parameter
β	dimensionless parameter
δ_m	Viscoelastic parameter
Z	Modified Hartman number
K	Material parameter
σ_s	Slip condition

The normalized velocity is $f'=\frac{u}{U_e}$, and the physical quantities in engineering applications are defined as:

$$C_f=\frac{\tau_w}{\rho U_e^2}, \qquad Nu_x=\frac{xq_w}{k\left(T_w-T_\infty\right)},$$

$$Sh_x=\frac{xJ_w}{D_m\left(C_w-C_\infty\right)}, \quad (22)$$

where C_f is the skin friction, Nu_x is the local Nusselt number and Sh_x is the local Sherwood number for transfer of mass. τ_w is the wall shear stress of MVMF, q_w is wall heat current, and J_w is wall mass current, which are defined as:

$$\tau_w=-\mu\left(1+\delta_m\right)\left[\left(1+K\right)\frac{\partial u}{\partial y}+KN\right]_{y=0}, \quad (23)$$

$$q_w=-k\left(\frac{\partial T}{\partial y}\right)_{y=0}, \qquad J_w=-D_m\left(\frac{\partial C}{\partial y}\right)_{y=0}. \quad (24)$$

Using similarity variables, we can obtain the non-dimensional engineering parameters as follows:

$$Re^{-\frac{1}{2}}C_f=-\left(1+\delta_m\right)\left(1+\frac{K}{2}\right)f''\left(0\right),$$

$$Re^{-\frac{1}{2}}Nu_x=-\theta'\left(0\right), \qquad Re^{-\frac{1}{2}}Sh_x=-\phi'\left(0\right), \quad (25)$$

where $Re=\frac{U_e x}{v}$ is the Reynolds number.

5. Numerical procedure

We decreased the higher order differential system within the initial value issue. The method of the numerical procedure is characterized underneath:

$$q\left(1\right)=f\left(\eta\right), \qquad q\left(2\right)=f'\left(\eta\right), \qquad q\left(3\right)=f''\left(\eta\right),$$

$$qq1=f'''\left(\eta\right), \qquad q\left(4\right)=R\left(\eta\right), \qquad q\left(5\right)=R'\left(\eta\right),$$

$$qq2=R''\left(\eta\right), \qquad q\left(6\right)=\theta\left(\eta\right), \qquad q\left(7\right)=\theta'\left(\eta\right),$$

$$qq3=\theta''\left(\eta\right), \qquad q\left(8\right)=\phi\left(\eta\right), \qquad q\left(9\right)=\phi'\left(\eta\right),$$

$$qq4=\phi''\left(\eta\right),$$

$$qq1=-\left(1+K-\delta_m q\left(1\right)q\left(1\right)\right)^{-1}\Big(q(1)q(3)$$
$$-q(2)q(2)-\delta_m\left(1-2q\left(1\right)q\left(2\right)q\left(3\right)\right)$$
$$+Kq\left(5\right)+Ze^{-dx}+1\Big),$$

$$qq2=-\left(1+\frac{K}{2}\right)^{-1}\Big(q\left(1\right)q\left(5\right)-q\left(2\right)q\left(4\right)$$
$$-K\left(2q\left(4\right)+q\left(3\right)\right)\Big),$$

$$qq3=-Pr\Big(q\left(1\right)q\left(7\right)+Duqq4+Gb\left(1+K\right)q\left(3\right)q\left(3\right)\Big),$$

$$qq4=Sc\left(q\left(1\right)q\left(9\right)+Srqq3\right),$$

$$q0\left(1\right);q0\left(2\right)-S-\sigma_s\left(1+\frac{K}{2}\right)q0\left(3\right);$$

$$q0\left(4\right)+\frac{q0\left(3\right)}{2};q0\left(6\right)-1;q0\left(8\right)-1;$$

$$qinf\left(2\right)-1;qinf\left(4\right);qinf\left(6\right);qinf\left(8\right).$$

6. Result and discussion

A numerical procedure known as the BVP4C strategy exposes the system of nonlinear ordinary differential conditions (Eqs. (15)–(18)) with regard to dimensionless boundary conditions (Eqs. (19)–(21)) to analyze the various physical parameters shown in Figures 2–9.

6.1. Multi-dependent Soret number

The Soret number, also known as thermophoresis, is a dimensionless number used to study the effect of temperature gradients on mass flux. The equation for the steady-state concentration field in hard-sphere particle suspensions is:

$$D_m \frac{\nabla C}{C} = -D_T \nabla T. \tag{26}$$

This shows the thermophoresis velocity of particles denoted by v_T, in which D_T is called "thermal diffusion coefficient" (Eqs. (26)–(28)). The Soret coefficient is defined as $S_T = \frac{D_T}{D_m}$ with dimension T^{-1} (Eqs. (27) and (28)). Along the moving particles, the sign of the Soret coefficient is visible. If $S_T > 0$, the particles show thermophobic behavior and if $S_T < 0$, they show thermophilic behavior. The experimental results for particle radii across the whole temperature range were fitted using the empirical expression of the Soret coefficient S_T, as follows:

$$S_T(T) = S_T^{\infty}\left[1 - exp\left(\frac{T^* - T}{T_0}\right)\right], \tag{27}$$

where S_T^{∞} is the reference value, T^* is the temperature, and T_0 is the strength of the temperature impacts.

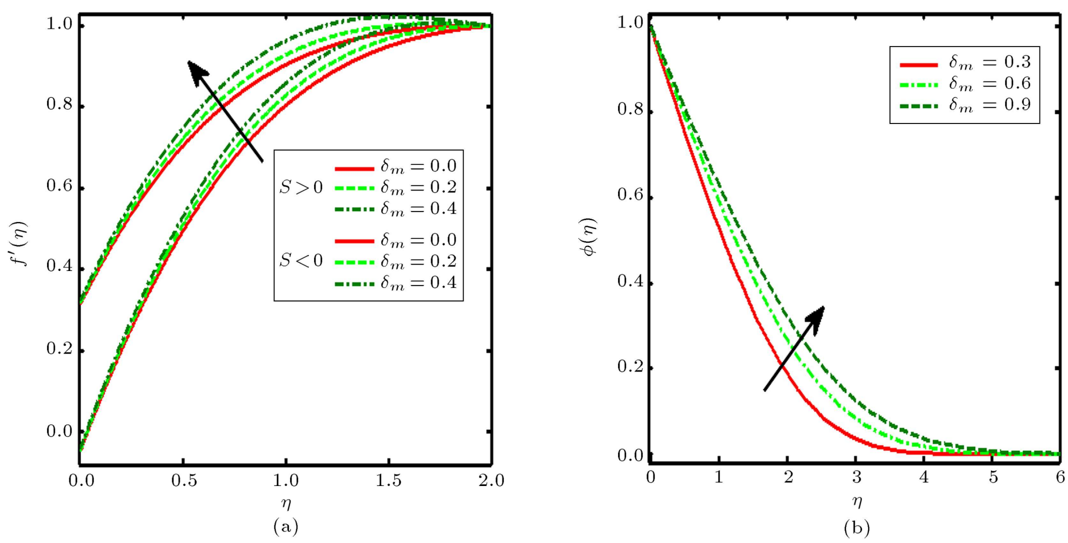

Figure 2. Effect of viscoelastic parameter δ_m on (a) normalized fluid velocity, and (b) concentration field ($Pr = 0.5$, $\sigma_s = 0.1$, $Du = 0.3$, $Sc = 0.2$, $Sr = 0.3$, $Ec = 0.3$, $K = 0.2$, $Z = 0.2$, $d = 0.2$, $S = -0.2, 0.2$).

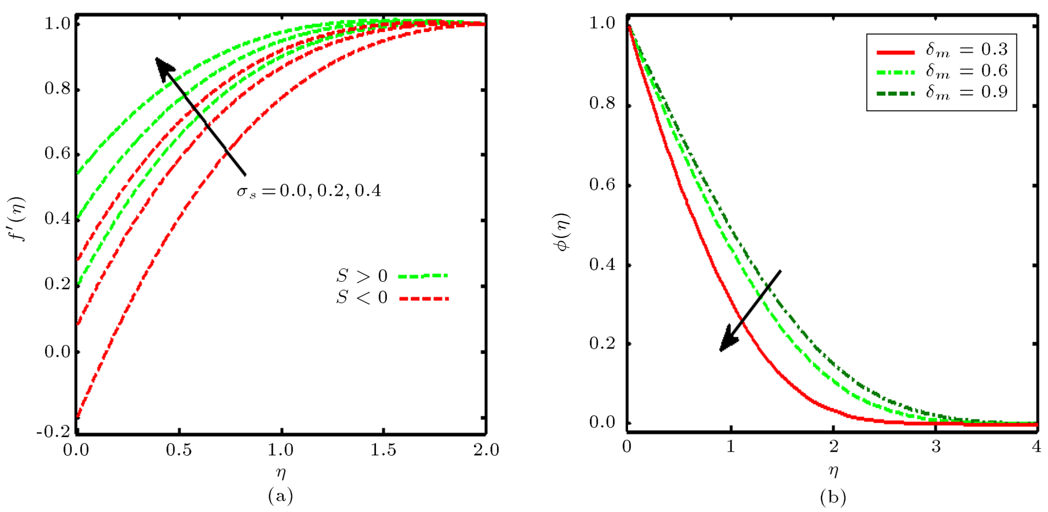

Figure 3. Effect of slip condition σ_s on (a) normalized fluid velocity, and (b) concentration field ($Pr = 0.5$, $\delta_m = 0.2$, $Du = 0.3$, $Sc = 0.2$, $Sr = 0.3$, $Ec = 0.3$, $K = 0.2$, $Z = 0.2$, $d = 0.2$, $S = -0.2, 0.2$).

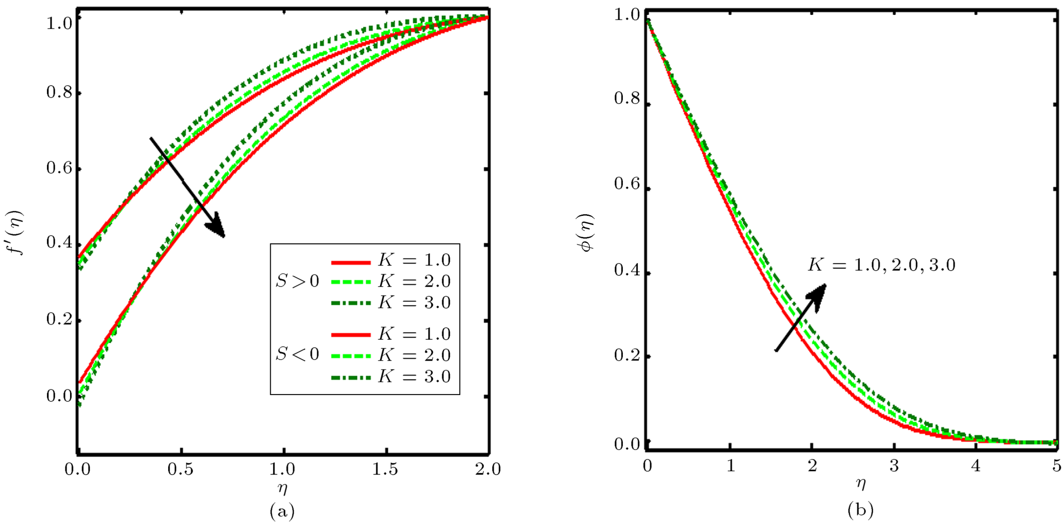

Figure 4. Effect of material parameter K on (a) normalized fluid velocity, and (b) concentration field ($Pr = 0.5$, $\delta_m = 0.2$, $\sigma_s = 0.1$, $Du = 0.3$, $Sc = 0.2$, $Sr = 0.3$, $Ec = 0.3$, $Z = 0.2$, $d = 0.2$, $S = -0.2, 0.2$).

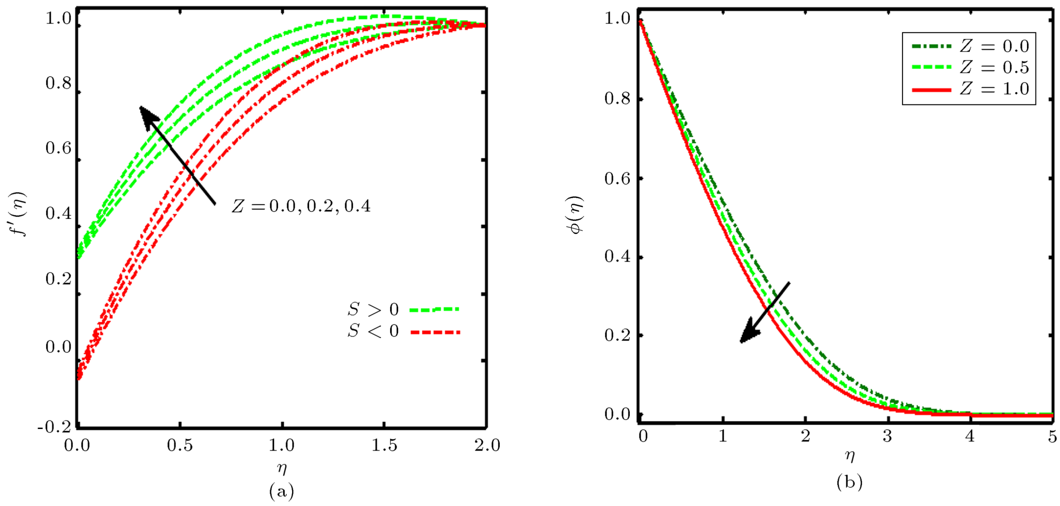

Figure 5. Effect of modified Hartman number Z on (a) normalized fluid velocity, and (b) concentration field ($Pr = 0.5$, $\delta_m = 0.2$, $\sigma_s = 0.1$, $Du = 0.3$, $Sc = 0.2$, $Sr = 0.3$, $Ec = 0.3$, $K = 0.2$, $Z = 0.2$, $S = -0.2, 0.2$).

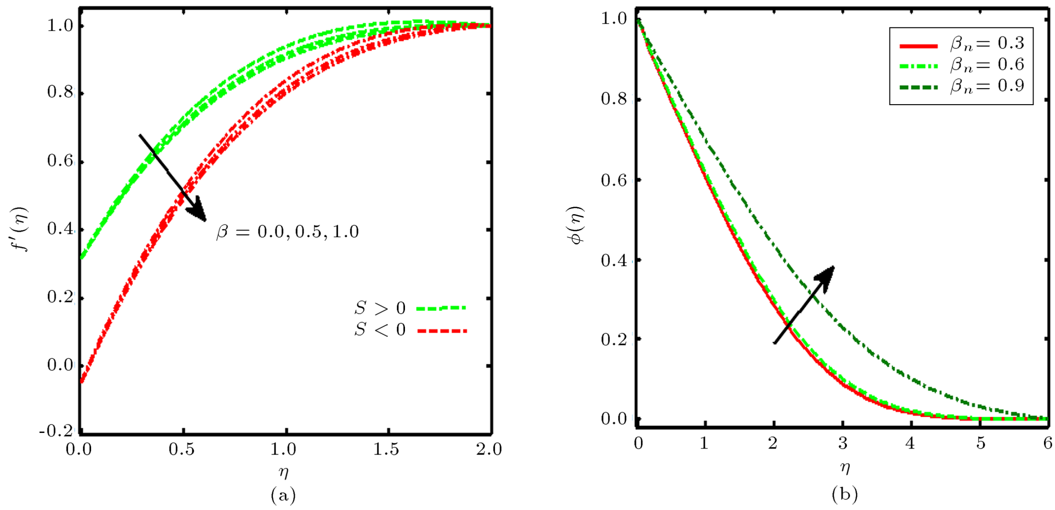

Figure 6. Effect of dimensionless parameter β on (a) normalized fluid velocity, and (b) concentration field ($Pr = 0.5$, $\delta_m = 0.2$, $\sigma_s = 0.1$, $Du = 0.3$, $Sc = 0.2$, $Sr = 0.3$, $Ec = 0.3$, $K = 0.2$, $Z = 0.2$, $S = -0.2, 0.2$).

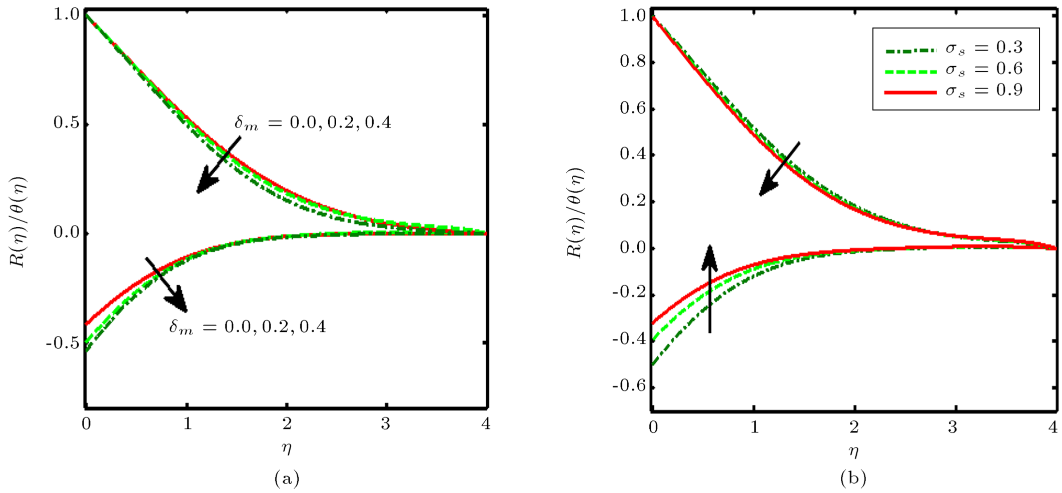

Figure 7. Effect of (a) viscoelastic parameter δ_m and (b) slip condition σ_s on $R(\eta)$ and $\theta(\eta)$ ($Pr = 0.5$, $\delta_m = 0.2$, $\sigma_s = 0.3$, $Du = 0.3$, $Sc = 0.2$, $Sr = 0.3$, $Ec = 0.3$, $K = 0.2$, $Z = 0.2$, $S = -0.2, 0.2$).

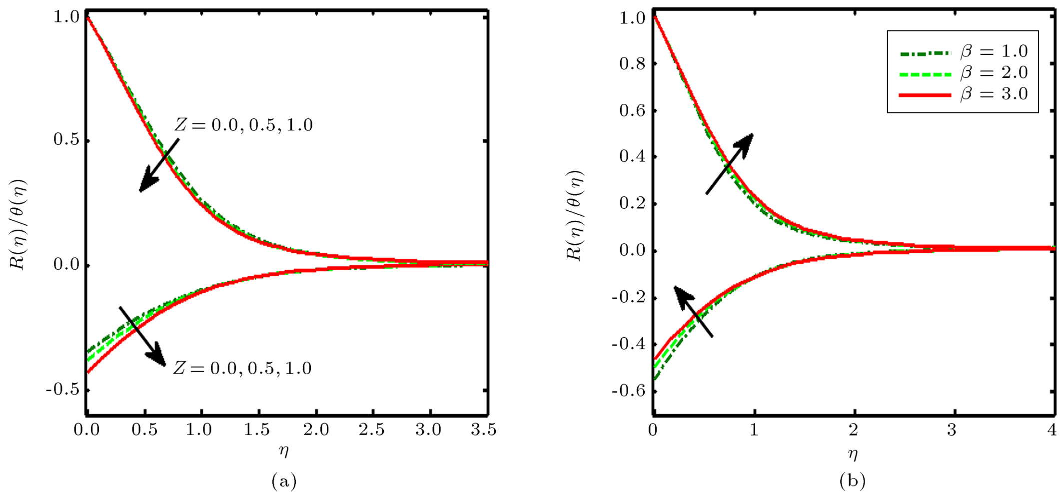

Figure 8. Effect of (a) modified Hartman number Z and (b) dimensionless parameter β on $R(\eta)$ and $\theta(\eta)$ ($Pr = 2.0$, $\delta_m = 0.5$, $\sigma_s = 0.5$, $Du = 0.3$, $Sc = 0.5$, $Sr = 0.3$, $Ec = 0.4$, $K = 0.5$, $Z = 2.0$, $S = 0.2$).

Here, we use multidependent Soret number Sr which is a functional equivalent of the Soret coefficient. We consider the case where $Sr\rangle 0$, then T^* and T_0 should be replaced by T_∞ and T_w, respectively. By transforming Eqs. (12) and (13) into Eq. (26) and gaining the variable Soret number, we will have:

$$Sr = Sr_\infty \left[1 - exp\left(\theta\left(\frac{T_\infty}{T_w} - 1\right)\right)\right], \tag{28}$$

where Sr_∞ is a positive coefficient and $0 < \frac{T_\infty}{T_w} < 1$ ensures $Sr > 0$. By using Eq. (27) in Eq. (18), we get:

$$\phi'' + Sc\Bigg(f\phi' + Sr_\infty\Bigg[1 - exp\left(\theta\left(\frac{T_\infty}{T_w} - 1\right)\right)\Bigg]\theta''\Bigg) = 0. \tag{29}$$

By solving Eqs. (15)–(21), the effects of normalized velocity, micro-angular velocity, temperature profile, and concentration profile, denoted by $f'(\eta), R(\eta), \theta(\eta)$ and $\phi(\eta)$, respectively will be examined.

6.2. Numerical results

The impacts of some physical quantities such as skin friction coefficients $Re^{\frac{1}{2}}C_f$, local Nusselt number $Re^{-\frac{1}{2}}Nu_x$, and local Sherwood number $Re^{-\frac{1}{2}}Sh_x$ are shown in Table 1. The effects of different parameters such as $S, K, \delta_m, \sigma_s, Du, Sc, Sr, Ec, Z$ and d on the alternance of physical quantities $Re^{\frac{1}{2}}C_f$, $Re^{-\frac{1}{2}}Nu_x$ and $Re^{-\frac{1}{2}}Sh_x$ are shown in Table 1. For stretching parameter ($S > 0$), the values of $Re^{\frac{1}{2}}C_f$, $Re^{-\frac{1}{2}}Nu_x$, and $Re^{-\frac{1}{2}}Sh_x$ increase, however, for ($S < 0$), the values of $Re^{\frac{1}{2}}C_f$ and $Re^{-\frac{1}{2}}Nu_x$ increase while $Re^{-\frac{1}{2}}Sh_x$ decreases. For large values of K, the values of $Re^{\frac{1}{2}}C_f$

and $Re^{-\frac{1}{2}}Nu_x$ decline whereas the values of $Re^{-\frac{1}{2}}Sh_x$ rise. The values of all physical quantities of $Re^{\frac{1}{2}}C_f$, $Re^{-\frac{1}{2}}Nu_x$ and $Re^{-\frac{1}{2}}Sh_x$ decrease with the increase of the values of δ_m. Both the values of $Re^{\frac{1}{2}}C_f$ and $Re^{-\frac{1}{2}}Nu_x$ decline while the values of $Re^{-\frac{1}{2}}Sh_x$ improve for larger values of Ec. For increasing values of Du and Sc, $Re^{\frac{1}{2}}C_f$, $Re^{-\frac{1}{2}}Nu_x$ and $Re^{-\frac{1}{2}}Sh_x$ show constant, decreasing, and increasing behavior, respectively. The behavior of $Re^{\frac{1}{2}}C_f$ and $Re^{-\frac{1}{2}}Nu_x$ is identical to that of Sr and σ_s whereas the behavior of $Re^{-\frac{1}{2}}Sh_x$ is fundamentally opposed to that of Sr and σ_s. The nature of $Re^{-\frac{1}{2}}Nu_x$ and $Re^{-\frac{1}{2}}Sh_x$ is the same as the nature of Z, however the nature of $Re^{\frac{1}{2}}C_f$ is opposite. The values of $Re^{\frac{1}{2}}C_f$ and $Re^{-\frac{1}{2}}Nu_x$ increase as the values of d increase but the values of $Re^{-\frac{1}{2}}Sh_x$ declines as the values of d increase.

The BVP4C numerical scheme is used to examine the physical parameters such as multi-dependent Soret number Sr_∞ and variable temperature difference $\frac{T_\infty}{T_w}$ in dimensionless systems (Eqs. (15)–(17) and (28)) with dimensionless boundary conditions (Eqs. (19)–(21)). The effect of different physical quantities such as skin friction, Nusselt number, and Sherwood number are shown in Table 2. The varia-

Table 1. Numerical values of skin friction, local Nusselt number and local Sherwood.

S	K	δ_m	σ_s	Du	Sc	Sr	Gb	Z	d	$Re^{\frac{1}{2}}C_f$	$Re^{-\frac{1}{2}}Nu_x$	$Re^{-\frac{1}{2}}Sh_x$
–0.3	0.6	0.4	0.5	0.3	0.5	0.4	0.3	0.7	0.9	–2.1853	0.4554	0.5422
–0.2	–	–	–	–	–	–	–	–	–	–2.0684	0.5306	0.5359
–0.1	–	–	–	–	–	–	–	–	–	–1.9627	0.5955	0.5342
0.0	–	–	–	–	–	–	–	–	–	–1.8563	0.6561	0.5335
0.1	–	–	–	–	–	–	–	–	–	–1.7497	0.7124	0.5337
0.2	–	–	–	–	–	–	–	–	–	–1.6276	0.7709	0.5307
0.3	0.0	–	–	–	–	–	–	–	–	–1.3274	0.8951	0.5027
–	0.3	–	–	–	–	–	–	–	–	–1.4279	0.8563	0.5188
–	0.6	–	–	–	–	–	–	–	–	–1.4892	0.8310	0.5243
–	0.9	–	–	–	–	–	–	–	–	–1.5595	0.8034	0.5331
–	0.6	0.0	–	–	–	–	–	–	–	–0.8180	0.8967	0.4346
–	–	0.2	–	–	–	–	–	–	–	–0.9403	0.7994	0.4317
–	–	0.4	–	–	–	–	–	–	–	–1.4892	0.8310	0.5243
–	–	0.4	0.0	–	–	–	–	–	–	–4.0139	–1.0615	0.9111
–	–	–	0.5	–	–	–	–	–	–	–1.4892	0.8310	0.5243
–	–	–	1.0	–	–	–	–	–	–	–1.1883	0.9440	0.5797
–	–	–	0.5	0.0	–	–	–	–	–	–1.4892	0.9121	0.5112
–	–	–	–	0.2	–	–	–	–	–	–1.4892	0.8594	0.5197
–	–	–	–	0.3	–	–	–	–	–	–1.4892	0.8310	0.5243
–	–	–	–	0.5	–	–	–	–	–	–3.1899	–0.3621	0.9832
–	–	–	–	0.3	0.2	–	–	–	–	–1.4892	0.8756	0.3579
–	–	–	–	–	0.3	–	–	–	–	–1.4892	0.8602	0.4228
–	–	–	–	–	0.5	–	–	–	–	–1.4892	0.8310	0.5243
–	–	–	–	–	1.0	–	–	–	–	–3.1899	–0.4175	1.4695
–	–	–	–	–	0.5	0.0	–	–	–	–3.1899	–0.1072	0.8330
–	–	–	–	–	–	0.2	–	–	–	–3.1899	–0.1447	0.8882
–	–	–	–	–	–	0.4	–	–	–	–1.4892	0.8310	0.5243
–	–	–	–	–	–	0.6	–	–	–	–1.4892	0.8467	0.4766
–	–	–	–	–	–	0.4	0.0	–	–	–1.4892	1.1020	0.4743
–	–	–	–	–	–	–	0.3	–	–	–1.4892	0.8310	0.5243
–	–	–	–	–	–	–	0.5	–	–	–3.1899	–1.2950	1.1511
–	–	–	–	–	–	–	0.3	0.0	–	–1.1808	0.8163	0.4878
–	–	–	–	–	–	–	–	0.3	–	–1.3217	0.8221	0.5055
–	–	–	–	–	–	–	–	0.7	–	–1.4892	0.8310	0.5243
–	–	–	–	–	–	–	–	0.7	0.0	–3.9920	–0.7724	1.1407
–	–	–	–	–	–	–	–	–	0.5	–1.6072	0.8078	0.5487
–	–	–	–	–	–	–	–	–	0.9	–1.4892	0.8310	0.5243
–	–	–	–	–	–	–	–	–	1.2	–1.4470	0.8338	0.5173

Table 2. Numerical values of skin friction, local Nusselt number and local Sherwood number.

S	$\frac{T_\infty}{T_w}$	Sr_∞	K	δ_m	σ_s	Du	Sc	Sr	Gb	Z	d	$Re^{\frac{1}{2}}C_f$	$Re^{-\frac{1}{2}}Nu_x$	$Re^{-\frac{1}{2}}Sh_x$
–0.3	0.6	0.8	0.6	0.4	0.5	0.3	0.5	0.4	0.3	0.7	0.9	–2.1853	0.4599	0.5843
–0.2	–	–	–	–	–	–	–	–	–	–	–	–2.0684	0.5352	0.5842
–0.1	–	–	–	–	–	–	–	–	–	–	–	–1.9627	0.6003	0.5877
0.0	–	–	–	–	–	–	–	–	–	–	–	–1.8563	0.6610	0.5919
0.1	–	–	–	–	–	–	–	–	–	–	–	–1.7497	0.7174	0.5967
0.2	–	–	–	–	–	–	–	–	–	–	–	–1.6276	0.7760	0.5988
0.3	0.0	–	–	–	–	–	–	–	–	–	–	–1.4892	0.8345	0.5779
–	0.3	–	–	–	–	–	–	–	–	–	–	–1.4892	0.8353	0.5878
–	0.6	–	–	–	–	–	–	–	–	–	–	–1.4892	0.8361	0.5980
–	0.8	–	–	–	–	–	–	–	–	–	–	–1.4892	0.8367	0.6049
–	0.6	0.0	–	–	–	–	–	–	–	–	–	–1.4892	0.8374	0.6117
–	–	0.4	–	–	–	–	–	–	–	–	–	–1.4892	0.8368	0.6049
–	–	0.8	–	–	–	–	–	–	–	–	–	–1.4892	0.8361	0.5980
–	–	1.0	–	–	–	–	–	–	–	–	–	–1.4892	0.8358	0.5945
–	–	0.8	0.0	–	–	–	–	–	–	–	–	–1.3274	0.9006	0.5840
–	–	–	0.3	–	–	–	–	–	–	–	–	–1.4279	0.8616	0.5954
–	–	–	0.6	–	–	–	–	–	–	–	–	–1.4892	0.8361	0.5980
–	–	–	0.9	–	–	–	–	–	–	–	–	–1.5595	0.8084	0.6033
–	–	–	0.6	0.0	–	–	–	–	–	–	–	–0.8180	0.9022	0.5202
–	–	–	–	0.2	–	–	–	–	–	–	–	–0.9403	0.8043	0.4992
–	–	–	–	0.4	–	–	–	–	–	–	–	–1.4892	0.8361	0.5980
–	–	–	–	0.4	0.0	–	–	–	–	–	–	–4.1749	–1.2211	0.9025
–	–	–	–	–	0.5	–	–	–	–	–	–	–1.4892	0.8361	0.5980
–	–	–	–	–	1.0	–	–	–	–	–	–	–1.1883	0.9492	0.6590
–	–	–	–	–	0.5	0.0	–	–	–	–	–	–1.4892	0.9121	0.5961
–	–	–	–	–	–	0.2	–	–	–	–	–	–1.4892	0.8629	0.5972
–	–	–	–	–	–	0.3	–	–	–	–	–	–1.4892	0.8361	0.5980
–	–	–	–	–	–	0.3	0.2	–	–	–	–	–1.4892	0.8768	0.3960
–	–	–	–	–	–	–	0.3	–	–	–	–	–1.4892	0.8624	0.4745
–	–	–	–	–	–	–	0.5	–	–	–	–	–1.4892	0.8361	0.5980
–	–	–	–	–	–	–	1.0	–	–	–	–	–1.4892	0.7749	0.8295
–	–	–	–	–	–	–	0.5	0.0	–	–	–	–3.1899	–0.1059	0.9325
–	–	–	–	–	–	–	–	0.2	–	–	–	–3.1899	–0.1422	0.9386
–	–	–	–	–	–	–	–	0.4	–	–	–	–1.4892	0.8361	0.5980
–	–	–	–	–	–	–	–	0.6	–	–	–	–1.4892	0.8554	0.5976
–	–	–	–	–	–	–	–	0.4	0.0	–	–	–1.4892	1.1080	0.5758
–	–	–	–	–	–	–	–	–	0.3	–	–	–1.4892	0.8361	0.5980
–	–	–	–	–	–	–	–	–	0.5	–	–	–3.1899	–1.2923	1.1021
–	–	–	–	–	–	–	–	–	0.3	0.0	–	–1.1808	0.8212	0.5595
–	–	–	–	–	–	–	–	–	–	0.3	–	–1.3217	0.8271	0.5779
–	–	–	–	–	–	–	–	–	–	0.7	–	–1.4892	0.8361	0.5980
–	–	–	–	–	–	–	–	–	–	0.7	0.0	–1.8173	0.7658	0.6580
–	–	–	–	–	–	–	–	–	–	–	0.5	–1.6072	0.8129	0.6197
–	–	–	–	–	–	–	–	–	–	–	0.9	–1.4892	0.8361	0.5980
–	–	–	–	–	–	–	–	–	–	–	1.2	–1.4470	0.8389	0.5911

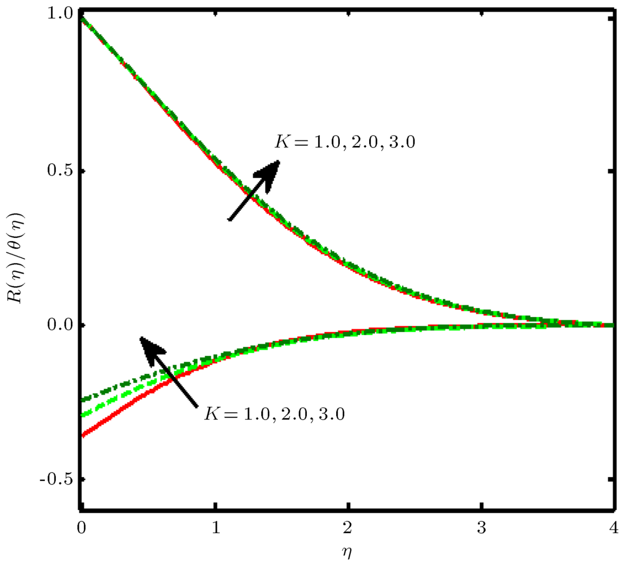

Figure 9. Effect of material parameter K on $R(\eta)$ and $\theta(\eta)$, ($Pr = 0.5$, $\delta_m = 0.2$, $\sigma_s = 0.3$, $Du = 0.3$, $Sc = 0.2$, $Sr = 0.3$, $Ec = 0.3$, $K = 0.2$, $Z = 0.2$, $S = 0.2$).

tion of $S, \frac{T_\infty}{T_w}, Sr_\infty, K, \delta_m, \sigma_s, Du, Sc, Sr, Ec, Z$ and d on $Re^{\frac{1}{2}}C_f$, $Re^{-\frac{1}{2}}Nu_x$, and $Re^{-\frac{1}{2}}Sh_x$ are shown in Table 2. For ($S > 0$), the values of $Re^{\frac{1}{2}}C_f$, $Re^{-\frac{1}{2}}Nu_x$ and $Re^{-\frac{1}{2}}Sh_x$ increase whereas for ($S < 0$), the values of $Re^{\frac{1}{2}}C_f$, and $Re^{-\frac{1}{2}}Nu_x$ increase while the values of $Re^{-\frac{1}{2}}Sh_x$ decrease for increasing values of S. The values of $Re^{-\frac{1}{2}}Nu_x$, and $Re^{-\frac{1}{2}}Sh_x$ increase for large values of $\frac{T_\infty}{T_w}$ whereas $Re^{\frac{1}{2}}C_f$ remains constant. The effects of Sr_∞ on $Re^{\frac{1}{2}}C_f$, $Re^{-\frac{1}{2}}Nu_x$, and $Re^{-\frac{1}{2}}Sh_x$ are shown in Table 2. It is evident that for higher values of Sr_∞, $Re^{-\frac{1}{2}}Nu_x$ and $Re^{-\frac{1}{2}}Sh_x$ show decreasing behavior whereas the values of $Re^{\frac{1}{2}}C_f$ remain constant. For increasing values of K, $Re^{\frac{1}{2}}C_f$ and $Re^{-\frac{1}{2}}Nu_x$ show decreasing behavior while $Re^{-\frac{1}{2}}Sh_x$ behaves in the opposite way, as shown in Table 2. The effects of δ_m on $Re^{\frac{1}{2}}C_f$, $Re^{-\frac{1}{2}}Nu_x$ and $Re^{-\frac{1}{2}}Sh_x$ are shown in Table 2. For large values of δ_m, $Re^{\frac{1}{2}}C_f$, $Re^{-\frac{1}{2}}Nu_x$ and $Re^{-\frac{1}{2}}Sh_x$ show decreasing behavior. The impacts of σ_s on $Re^{\frac{1}{2}}C_f$, $Re^{-\frac{1}{2}}Nu_x$, and $Re^{-\frac{1}{2}}Sh_x$ are shown in Table 2. It is perceived that the values of $Re^{\frac{1}{2}}C_f$ and $Re^{-\frac{1}{2}}Nu_x$ rise in response to rising behavior of σ_s while the values of $Re^{-\frac{1}{2}}Sh_x$ show opposite behavior that decreases for large values of σ_s. Table 2 shows the effects of Du and Sc on $Re^{\frac{1}{2}}C_f$, $Re^{-\frac{1}{2}}Nu_x$, and $Re^{-\frac{1}{2}}Sh_x$. As is shown, the behavior of $Re^{\frac{1}{2}}C_f$ is constant while $Re^{-\frac{1}{2}}Nu_x$, and $Re^{-\frac{1}{2}}Sh_x$ show opposite behavior to each other and $Re^{-\frac{1}{2}}Nu_x$ decreases and $Re^{-\frac{1}{2}}Sh_x$ increases for increasing values of Du and Sc. For large values of Sr, the behavior of $Re^{\frac{1}{2}}C_f$, $Re^{-\frac{1}{2}}Nu_x$, and $Re^{-\frac{1}{2}}Sh_x$ is shown in Table 2. Also $Re^{\frac{1}{2}}C_f$ and $Re^{-\frac{1}{2}}Nu_x$ increase whereas $Re^{-\frac{1}{2}}Sh_x$ declines for great values of Sr. Table 2 depicts the impacts of Gb on physical quantities of $Re^{\frac{1}{2}}C_f$, $Re^{-\frac{1}{2}}Nu_x$, and $Re^{-\frac{1}{2}}Sh_x$. For increasing behavior of Gb, $Re^{\frac{1}{2}}C_f$ and $Re^{-\frac{1}{2}}Nu_x$ show decreasing behavior, while $Re^{-\frac{1}{2}}Sh_x$ shows increasing behavior. Table 2 shows the effects of Z on $Re^{\frac{1}{2}}C_f$, $Re^{-\frac{1}{2}}Nu_x$, and $Re^{-\frac{1}{2}}Sh_x$. It is observed that both $Re^{-\frac{1}{2}}Nu_x$, and $Re^{-\frac{1}{2}}Sh_x$ increase whereas $Re^{\frac{1}{2}}C_f$ decreases for rising values of Z. The values of $Re^{\frac{1}{2}}C_f$ and $Re^{-\frac{1}{2}}Nu_x$ surge for higher values of d however the values of $Re^{-\frac{1}{2}}Sh_x$ decreases as shown in Table 2.

6.3. Graphical results

Figures 2–11 shows the effects of different physical parameters, such as dimensionless parameter β, modified Hartman number Z, material parameter K, slip condition σ_s, viscoelastic parameter δ_m, multi dependent Soret number Sr_∞, and variable temperature difference $\frac{T_\infty}{T_w}$, on normalized fluid velocity $\left(\frac{u}{U_e}\right)$, micro-angular velocity (R), temperature profile (θ) and concentration profile (ϕ). Figure 2(a) and (b) demonstrate the impact of viscoelastic parameter δ_m on $f' = \frac{u}{U_e}$ and ϕ. Both f' and ϕ increase in response to the increase in the values of the viscoelastic parameter δ_m. Figure 3(a) and (b) depict the impact of the slip condition σ_s on f' and ϕ, respectively. It should be noted that f' increases as well as ϕ decreases in response to increasing values of slip condition σ_s. Figure 4(a) and (b) show the impact of the material parameter K on f' and ϕ, respectively. For increase in material parameter, f' has decreasing behavior whereas ϕ has increasing behavior. Figure 5(a) and (b) show the impact of Hartman number Z on f' and ϕ. As the Hartman number Z increases, f' increases while ϕ decreases. Figure 6(a) and (b) depict the impacts of dimensionless parameter β on f' and ϕ. It is observed that f' displays decreasing behavior and ϕ shows increasing behavior for large values of the dimensionless parameter β. Figure 7(a) and (b) show the impact of viscoelastic parameter δ_m and slip condition σ_s on R and θ, respectively. It is observed that R declines in response to the rise of σ_s and increases in response to the increase in δ_m while θ decreases for both viscoelastic parameters of δ_m and slip condition σ_s. The effects of modified Hartman number Z on R and θ are shown in Figure 8(a). For higher values of Z, it is observed that R increases and θ decreases. Figure 8(b) depicts the effects of dimensionless parameter β on R and θ. It is noted that R and θ show opposite behavior that R decreases and θ increases. Figure 9 shows the impact of material parameter K on R and θ. It is also observed that θ shows the same behavior as K whereas R shows the opposite. Figure 10 depicts the effect of multi-dependent Soret number Sr_∞ on ϕ. It is observed that ϕ increases when the multi-dependent Soret number increases. The effect of the variable

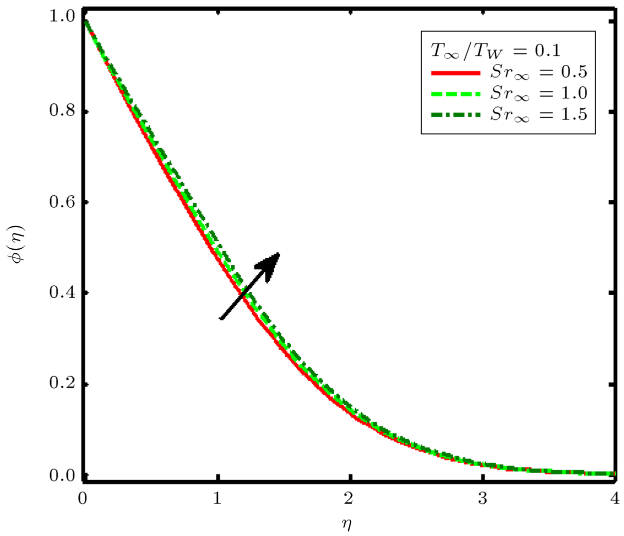

Figure 10. The parameter Sr_∞ associated with the micro-particle size has visible effect on the concentration field with large imposed temperature differences $\frac{T_\infty}{T_w}$. ($Pr = 2.0$, $\delta_m = 0.5$, $\sigma_s = 0.5$, $Du = 0.3$, $Sc = 0.5$, $Sr = 0.3$, $Ec = 0.4$, $K = 0.5$, $Z = 1.0$, $S = 0.2$).

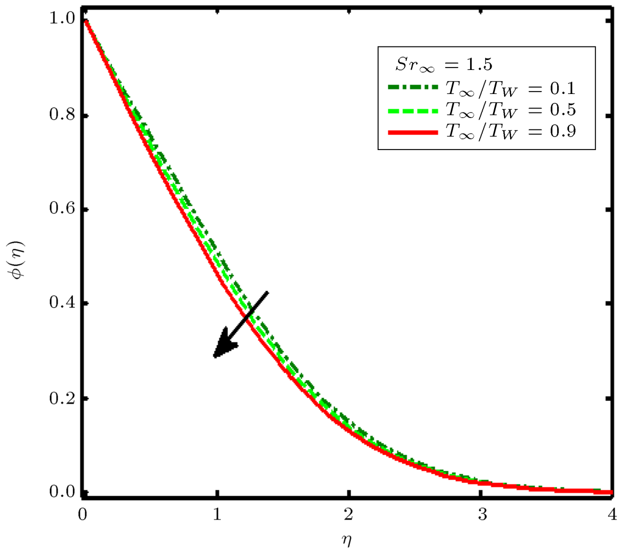

Figure 11. Effect of variable temperature differences $\frac{T_\infty}{T_w}$ on the concentration field of large particle ($Pr = 2.0$, $\delta_m = 0.5$, $\sigma_s = 0.5$, $Du = 0.3$, $Sc = 0.5$, $Sr = 0.3$, $Ec = 0.4$, $K = 0.5$, $Z = 1.0$, $S = 0.2$).

temperature difference $\frac{T_\infty}{T_w}$ on ϕ is shown in Figure 11. It should be noted that the concentration profile and the variable temperature difference showed the opposite behavior.

7. Conclusions

In this paper, we investigated the two-dimensional Maxwell viscoelasticity-based micropolar fluid (MVMF) in the stagnation point over a horizontal Riga plate with slip velocity condition. We also studied the impacts of different physical parameters and showed the results of these parameters. Some significant results are given below:

- With the increase of the dimensionless parameter β and material parameter K, θ and ϕ increased;
- θ and ϕ decreased for increased values of slip condition σ_s and modified Hartman number Z;
- R increased with the increase of the dimensionless parameter β, material parameter K, and slip condition σ_s;
- R decreased with increasing behavior of the modified Hartman number Z and the viscoelastic parameter δ_m.

References

1. Lukaszewicz, G., *Micropolar Fluids: Theory and Applications*, Springer Science & Business Media (1999).
2. Eringen, A.C., *Microcontinuum Field Theories: II. Fluent Media*, (**2**) Springer Science & Business Media (2001).
3. Wang, X.L. and Zhu, K.Q. "A study of the lubricating effectiveness of micropolar fluids in a dynamically loaded journal bearing (T1516)", *Tribology International*, **37**(6), pp. 481–490 (2004).
4. Nadeem, S., Akbar, N.S., and Malik, M.Y. "Exact and numerical solutions of a micropolar fluid in a vertical annulus", *Numerical Methods for Partial Differential Equations*, **26**(6), pp. 1660–1674 (2010).
5. Hussain, S.T., Nadeem, S., and Haq, R.U. "Model-based analysis of micropolar nanofluid flow over a stretching surface", *The European Physical Journal Plus*, **129**(8), p. 161 (2014).
6. Ellahi, R., Rahman, S.U., Nadeem, S., and Akbar, N.S. "Influence of heat and mass transfer on micropolar fluid of blood flow through a tapered stenosed arteries with permeable walls", *Journal of Computational and Theoretical Nanoscience*, **11**(4), pp. 1156–1163 (2014).
7. Rawi, N.A., Ilias, M.R., Isa, Z.M., and Shafie, S. "G-Jitter induced mixed convection flow and heat transfer of micropolar nanofluids flow over an inclined stretching sheet", In *AIP Conference Proceedings* **1775**(1), p. 030020, AIP Publishing (2016).
8. Abbas, N., Saleem, S., Nadeem, S., Alderremy, A.A., and Khan, A.U. "On stagnation point flow of a micro polar nanofluid past a circular cylinder with velocity and thermal slip", *Results in Physics*, **9**, pp. 1224–1232 (2018).
9. Nadeem, S., Malik, M.Y., and Abbas, N. "Heat transfer of three dimensional micropolar fluids on Riga plate", *Canadian Journal of Physics*, **98**(1), pp. 32-38 (2020).

10. Mollamahdi, M., Abbaszadeh, M., and Sheikhzadeh, G.A. "Analytical study of Al2O3-Cu/water micropolar hybrid nanofluid in a porous channel with expanding/contracting walls in the presence of magnetic field", *Scientia Iranica*, **25**(1), pp. 208–220 (2018).

11. Nayak, M.K., Zeeshan, A., Pervaiz, Z., and Makinde, O.D., "Modelling, measurement and control B", **88**(1), pp. 33–41 (2019).

12. Abro, K.A. and Yildirim, A. "An analytic and mathematical synchronization of micropolar nanofluid by Caputo-Fabrizio approach", *Scientia Iranica*, **26**(6), pp. 3917–3927 (2019).

13. Atif, S.M., Hussain, S., and Sagheer, M. "Effect of thermal radiation on MHD micropolar Carreau nanofluid with viscous dissipation, Joule heating, and internal heating", *Scientia Iranica, Transactions F, Nanotechnology*, **26**(6), pp. 3875–3888 (2019).

14. Gailitis, A.K. and Lielausis, O.A. "On the possibility of drag reduction of a flat plate in an electrolyte", *Appl. Magnetohydrodyn. Trudy Inst. Fisiky AN Latvia SSR*, **12**, p. 143 (1961).

15. Grinberg, E. "On determination of properties of some potential fields", *Applied Magnetohydrodynamics Reports of the Physics Institute*, **12**, pp. 147–154 (1961).

16. Pantokratoras, A. and Magyari, E. "EMHD free-convection boundary-layer flow from a Riga-plate", *Journal of Engineering Mathematics*, **64**(3), pp. 303–315 (2009).

17. Magyari, E. and Pantokratoras, A. "Aiding and opposing mixed convection flows over the Riga-plate", *Communications in Nonlinear Science and Numerical Simulation*, **16**(8), pp. 3158–3167 (2011).

18. Ayub, M., Abbas, T., and Bhatti, M.M. "Inspiration of slip effects on electromagnetohydrodynamics (EMHD) nanofluid flow through a horizontal Riga plate", *The European Physical Journal Plus*, **131**(6), p. 193 (2016).

19. Ramzan, M., Bilal, M., and Chung, J.D. "Radiative Williamson nanofluid flow over a convectively heated Riga plate with chemical reaction - A numerical approach", *Chinese Journal of Physics*, **55**(4), pp. 1663–1673 (2017).

20. Zaib, A., Haq, R.U., Chamkha, A.J., and Rashidi, M.M. "Impact of partial slip on mixed convective flow towards a Riga plate comprising micropolar TiO2-kerosene/water nanoparticles", *International Journal of Numerical Methods for Heat and Fluid Flow*, **29**(5), pp. 1647-1662 (2018).

21. Rasool, G. and Zhang, T. "Characteristics of chemical reaction and convective boundary conditions in Powell-Eyring nanofluid flow along a radiative Riga plate", *Heliyon*, **5**(4), e01479 (2019).

22. Bhatti, M.M., Zeeshan, A., Ellahi, R., and Shit, G.C. "Mathematical modeling of heat and mass transfer effects on MHD peristaltic propulsion of two-phase flow through a Darcy-Brinkman-Forchheimer porous medium", *Advanced Powder Technology*, **29**(5), pp. 1189–1197 (2018).

23. Nayak, M.K., Shaw, S., Makinde, O.D., and Chamkha, A.J. "Effects of homogenous-heterogeneous reactions on radiative NaCl-CNP nanofluid flow past a convectively heated vertical Riga plate", *Journal of Nanofluids*, **7**(4), pp. 657–667 (2018).

24. Mehmood, R., Nayak, M.K., Akbar, N.S., and Makinde, O.D. "Effects of thermal-diffusion and diffusion-thermo on oblique stagnation point flow of couple stress Casson fluid over a stretched horizontal Riga plate with higher order chemical reaction", *Journal of Nanofluids*, **8**(1), pp. 94–102 (2019).

25. Nayak, M.K., Shaw, S., Makinde, O.D., and Chamkha, A.J. "Investigation of partial slip and viscous dissipation effects on the radiative tangent hyperbolic nanofluid flow past a vertical permeable Riga plate with internal heating: Bungiorno model", *Journal of Nanofluids*, **8**(1), pp. 51–62 (2019).

26. Riaz, A., Ellahi, R., Bhatti, M.M., and Marin, M. "Study of heat and mass transfer on eyring-powell fluid model propagating peristaltically through a rectangular complaint channel", *Heat Transfer Research*, **50**(16), pp. 1539–1560 (2019)
DOI: 10.1615/HeatTransRes.2019025622

27. Khan, A.A., Bukhari, S.R., Marin, M., and Ellahi, R. "Effects of chemical reaction on third-grade MHD fluid flow under the influence of heat and mass transfer with variable reactive index", *Heat Transfer Research*, **50**(11), pp. 1061–1080 (2019).

28. Hiemenz, K. "Die Grenzschicht an einem in den gleichformigen Flussigkeitsstrom eingetauchten geraden Kreiszylinder", *Dinglers Polytech. J.*, **326**, pp. 321–324 (1911).

29. Howarth, L. "The boundary layer in three dimensional flow-Part II The flow near a stagnation point", *The London, Edinburgh, and Dublin Philosophical Magazine and Journal of Science*, **42**(335), pp. 1433-1440, (1951).

30. Ishak, A., Jafar, K., Nazar, R., and Pop, I. "MHD stagnation point flow towards a stretching sheet", *Physica A: Statistical Mechanics and Its Applications*, **388**(17), pp. 3377–3383 (2009).

31. Van Gorder, R.A. and Vajravelu, K. "Hydromagnetic stagnation point flow of a second grade fluid over a stretching sheet", *Mechanics Research Communications*, **37**(1), pp. 113–118 (2011).

32. Fang, T., Chia-fon, F.L., and Zhang, J. "The boundary layers of an unsteady incompressible stagnation-point flow with mass transfer", *International Journal of Non-Linear Mechanics*, **46**(7), pp. 942–948 (2011).
33. Nadeem, S., Abbas, N., and Khan, A.U. "Characteristics of three dimensional stagnation point flow of hybrid nanofluid past a circular cylinder", *Results in Physics*, **8**, pp. 829–835 (2018).
34. Nadeem, S. and Abbas, N. "On both MHD and slip effect in Micropolar hybrid nanofluid past a circular cylinder under stagnation point region", *Canadian Journal of Physics*, **97**(4), pp. 392–399 (2018).
35. Iacopini, S. and Piazza, R. "Thermophoresis in protein solutions", *EPL (Europhysics Letters)*, **63**(2), p. 247 (2003).
36. Putnam, S.A., Cahill, D.G., and Wong, G.C. "Temperature dependence of thermodiffusion in aqueous suspensions of charged nanoparticles", *Langmuir*, **23**(18), pp. 9221–9228 (2007).
37. Braibanti, M., Vigolo, D., and Piazza, R. "Does thermophoretic mobility depend on particle size", *Physical Review Letters*, **100**(10), p. 108303 (2008).
38. Khan, A.A., Usman, H., Vafai, K., and Ellahi, R. "Study of peristaltic flow of magnetohydrodynamics Walter's B fluid with slip and heat transfer", *Scientia Iranica*, **23**(6), pp. 2650–2662 (2016).
39. Niranjan, H., Sivasankaran, S., and Bhuvaneswari, M. "Chemical reaction, Soret and Dufour effects on MHD mixed convection stagnation point flow with radiation and slip condition", *Scientia Iranica, Transactions B, Mechanical Engineering*, **24**(2), p. 698 (2017).
40. Ijaz, N., Zeeshan, A., Bhatti, M.M., and Ellahi, R. "Analytical study on liquid-solid particles interaction in the presence of heat and mass transfer through a wavy channel", *Journal of Molecular Liquids*, **250**, pp. 80–87 (2018).
41. Nayak, M.K., Hakeem, A.K., and Makinde, O.D. "Influence of Catteneo-Christov heat flux model on mixed convection flow of third grade nanofluid over an inclined stretched Riga plate", In *Defect and Diffusion Forum*, **387**, pp. 121–134, Trans Tech Publications Ltd (2018).

Biographies

Sohail Nadeem is working as Professor/Chairman at the Department of Mathematics at Quaid-i-Azam University, Islamabad, Pakistan. More than 25 PhD scholars and more than 100 MPhil students have completed their respective degrees under his supervision. He has published more than 500 research articles in well reputed international journals having more than 7000 citations. He has been awarded several national/international awards. He is also a member of several editorial boards in well reputed international journals. Nationally, he is serving on several scientific committees throughout the country.

Asma Amin was born in Rawalpindi, Punjab, Pakistan. He obtained his MPhil degrees from the Department of Mathematics at Quaid-iAzam University, Islamabad, Pakistan, and is currently working as a lecturer in the Department of Mathematics at HITEC University, Taxila Cantt, Rawalpindi, Punjab, Pakistan. She published her work in the international well-reputed impact factor journal.

Nadeem Abbas was born on September 15, 1990, in District Jhang, Punjab, Pakistan. He earned his MS degree in Mathematics in 2014 from the University of the Punjab Lahore, Pakistan, and an MPhil and PhD degree from Quaid-i-Azam University Islamabad, Pakistan. Now, he is working as an Assistant Professor in the Department of Mathematics, Riphah International University, Faisalabad Campus, Faisalabad, Pakistan. He has published more than 30 research articles in well reputed international journals, having more than 470 citations.

Anber Saleem is working as Professor at the Department of Islamabad Medical and Dental College, Islamabad, Pakistan. She has published more than 50 research articles in well reputed international journals, having more than 500 citations. She is also a member of several editorial boards in well reputed international journals. Nationally, he is serving on several scientific committees throughout the country.

Fahad M. Alharbi is working as an Assistant Professor in the Department of Mathematics, Faculty of Science, University of Tabuk, Tabuk, Saudi Arabia. Nationally, he is serving on several scientific committees throughout the country. He has published more than 50 research articles in well reputed international journals, having more than 500 citations. He has been awarded several national/international awards. He is also a member of several editorial boards in well reputed international journals.

Anwar Hussain is working as an Assistant Professor in the Department of Mathematics, Quaid-i-Azam University Islamabad, Pakistan. Nationally, he is serving on several scientific committees throughout the country. He has published more than 40 research articles in well reputed international journals, having more than 500 citations. He has been awarded several national/international awards. Nationally, he is serving on several scientific committees throughout the country.

Alibek Issakhov Alharbi is working as a Professor in the Department of Mathematics Al-Farabi Kazakh National University, av. al-Farabi, Almaty, Kazakhstan. Nationally, he is serving on several scientific committees throughout the country. He has published more than 25 research articles in well reputed international journals, having more than 1000 citations. He has been awarded several national/international awards. He is also a member of several editorial boards in well reputed international journals.